SCIENCE CHINA
Physics, Mechanics & Astronomy

• Article •

March 2016 Vol. 59 No. 3: 634602
doi: 10.1007/s11433-015-5754-8

Effects of oxygen vacancies on polarization stability of barium titanate

Jun Wang[1], YaoGen Shen[2], Fan Song[1], FuJiu Ke[3*], YiLong Bai[1], and ChunSheng Lu[4]

[1] *State Key Laboratory of Nonlinear Mechanics (LNM), Institute of Mechanics, Chinese Academy of Sciences, Beijing 100190, China;*
[2] *Department of Mechanical and Biomedical Engineering, City University of Hong Kong, Hong Kong, China;*
[3] *School of Physics and Nuclear Energy Engineering, Beihang University, Beijing 100191, China;*
[4] *Department of Mechanical Engineering, Curtin University, Perth WA 6845, Australia*

Received July 15, 2015; accepted October 8, 2015

Oxygen vacancy, a kind of native point defects in ferroelectric ceramics, usually causes an increase of the dielectric loss. Based on experimental observations, it is believed that all of the oxygen vacancies are an unfavorable factor for energy saving. By using molecular dynamics simulations, we show that the increase of coercive and saturated electric fields is due to the difficulty to switch local polarization near an oxygen vacancy, and so that a ferroelectric device has to sustain the rising consumption of energy. The simulation results also uncover how oxygen vacancies influence ferroelectric properties.

ferroelectricity, hysteresis, oxygen vacancy, molecular dynamics simulation

PACS number(s): 77.80.-e, 77.80.Dj, 61.72.-y, 61.72.J-, 31.15.xv

Citation: J. Wang, Y. G. Shen, F. Song, F. J. Ke, Y. L. Bai, and C. S. Lu, Effects of oxygen vacancies on polarization stability of barium titanate, Sci. China-Phys. Mech. Astron. **59**, 634602 (2016), doi: 10.1007/s11433-015-5754-8

1 Introduction

Ferroelectric ceramics such as barium titanate (BTO) and lead zirconate titanate have attracted considerable interest over the last decade due to their excellent physical, optical and electrical properties. They have also had a great deal of applications in the fields of microactuators, nanogenerators, capacitors and memories [1-4]. All these remarkable properties are based on a unique feature of ferroelectric ceramics that can spontaneously polarize below a certain temperature, i.e., the Curie temperature [5]. Affected by an applied external electric field, the polarization intensity of a ferroelectric material always exhibits a lag phenomenon. As the electric field periodically changes, there is an electric hysteresis loop between the polarization intensity and electric field. Here, the hysteresis loop determines several key macroscopic properties of a material such as the remnant polarization, the saturated field and the coercive field [5]. Most importantly, the loop area (known as dielectric loss) represents the energy consumption per unit volume of a ferroelectric device during a working cycle, which is therefore the first concern in design of energy saving devices.

Extrinsic circumstance and inherent structure affect physical properties of a ferroelectric object. For example, a change of 0.5% in applied strain can cause a variation of 20% in the remnant polarization of BTO [1]. Oxygen vacancy (OV), a kind of native point defects, is inevitable in ferroelectric ceramics [6,7]. First-principles studies have revealed that the relative site of an OV with respect to the spontaneous polarization orientation has significant impact on the local polarization structure. Moreover this structure may be tuned by strain [8,9]. It has also been confirmed that dielectric loss increases with the increase of the OV concentration [10,11]. To the best of our knowledge, however,

*Corresponding author (email: kefj@lnm.imech.ac.cn)

micromechanism of OV behind the exceptional dielectric loss remains largely unexplored due to lack of an effective protocol for experiments. In this paper, by taking BTO as an example, a molecular dynamics study is performed to ascertain this issue from the atomistic perspective.

2 Method

To investigate ferroelectric behaviors of BTO, an isotropic core-shell model is developed based on the first-principles theory [12,13]. In the model, ions in a perovskite cell consist of a positively charged core and a negatively charged shell. The core and shell are connected with an inharmonic spring. Furthermore, the cell deformation can cause separation of its positive and negative charge centers, leading to spontaneous polarization of the cell. Thus, a cell that contributes a dipole is regarded as the smallest unit of a domain (see Figure 1(a) generated by the visual molecular dynamics [14]). The simulation box contains 16×16×16 cells with x, y and z coordinates along [100], [010] and [001] orientations, respectively. As illustrated in Figure 1(b), an OV is introduced by removing an oxygen ion and its corresponding charge. In this study, the nominal concentration of stochastically generated OVs varies from 0 to 2.4×10^{-2} at.%. In a perovskite cell, there are two relative sites for an OV: one is at the Ti-O chain along the spontaneous polarization orientation and the other on the TiO plane vertical to this direction [8,9]. Here, it is worth noting that OVs at the two sites lead to various local domain structures, which may have unexpected impact on switching behaviors. Thus, to focus on the influence of concentration, sites of OVs are confined to the TiO plane. To integrate the motion of shells, an adiabatic dynamics, in which a small mass is assigned to a shell, is carried out by using the DLPLOY package [15]. The temperature is set to 300 K, at which BTO adopts the tetragonal phase with spontaneous polarization along the [001] orientation. To allow fluctuations of the cell angle and length, the simulation system is contacted with an anisotropic Nosé-Hoover barostat [16,17]. The system pressure remains at zero to eliminate the effect of stress (or strain). The Coulomb interactions are calculated by the Wolf sum [18]. The applied external electric field E along the z direction ranges from -10×10^7 to 10×10^7 V/m with an increment of 0.25×10^7 V/m. The total time taken for applying an electric field is 20 ps with a time step of 0.4 fs. The system polarization $\bar{P}_z$ can be determined by averaging the local polarization P_z [19].

3 Results

As shown in Figure 2, it is obvious that an OV has a significant influence on the hysteresis loop of BTO. Specifically, as the OV concentration increases from 0 to 4.9×10^{-3} at.%, the remnant polarization $\bar{P}_{zr}$ decreases from 22.8 to 22.0 μC/cm^2. On the contrary, the saturated electric field E_s exhibits an increase of 33% from 4.5×10^7 to 6.0×10^7 V/m and the change of the coercive field E_c can be negligible. Analysis on switching of local polarization indicates that hot spots emerge before the formation of inverted domains (see Figure 3). Here, hot spots refer to regions with local polarization tending to switch inversely. It is worth noting that, however, the first hot spot might not be the one to firstly finish switching. For a single crystal system, the first hot spot appears at E=1.75×10^7 V/m. With E further increasing, more hot spots are initiated and subsequently evolve to inverted domains. These domains switch immediately as E increases to 3×10^7 V/m that is close to E_c=2.9×10^7 V/m. Finally, saturation is reached as E grows to 4.5×10^7 V/m. For the system with an OV, E=0.25×10^7 V/m should be high enough to trigger the first hot spot. However, as E increases to 4.5×10^7 V/m, the domains near the OV still remain unswitched.

Ferroelectric properties of BTO versus the concentration of OVs are summarized in Figure 4. It is seen that as the OV concentration increases from 0 to 2.4×10^{-2} at.%, the rem-

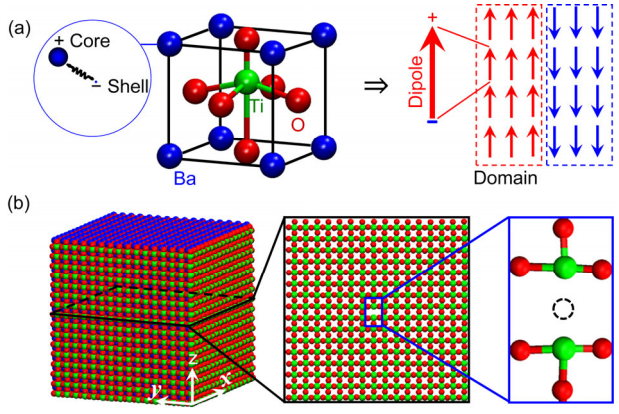

Figure 1 (Color online) Illustrations of (a) a core shell model and (b) a simulating box, where the dashed circle represents an OV.

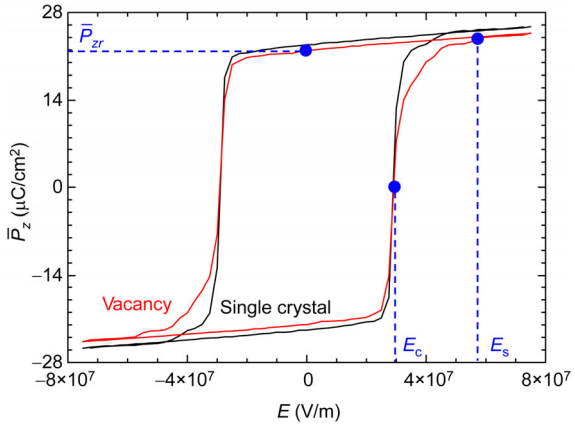

Figure 2 (Color online) The hysteresis loop of a single crystal in contrast to that of a system with an OV.

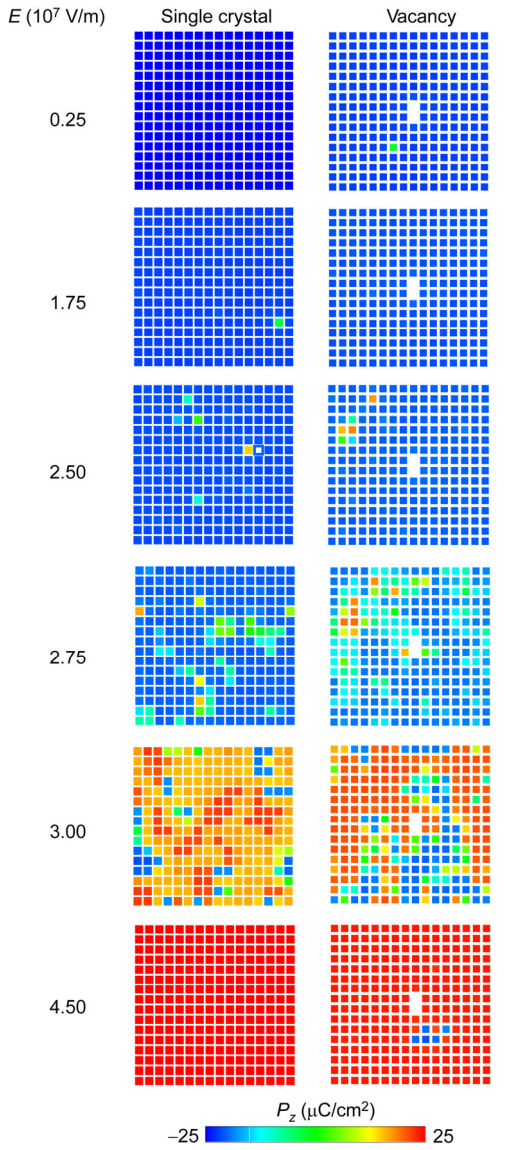

Figure 3 (Color Online) Evolving patterns of local polarization with the increase of *E*.

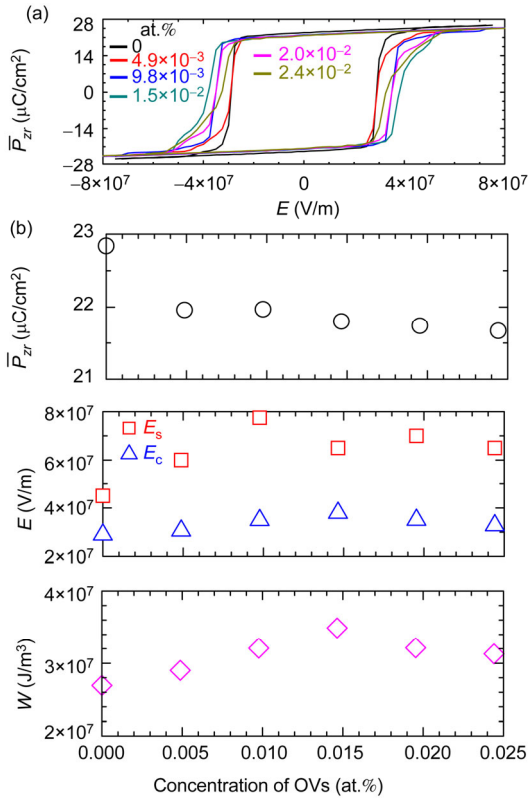

Figure 4 (Color online) (a) Hysteresis loops and (b) ferroelectric properties of BTO versus the concentration of OVs.

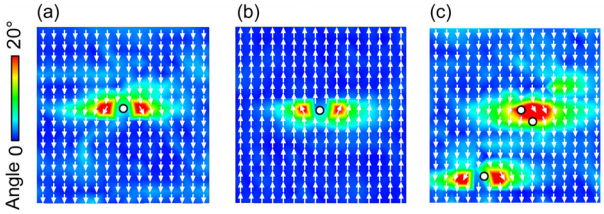

Figure 5 (Color online) The angle distribution of local polarization, where (a) and (b) are patterns of an isolated OV and (c) is the interaction of OVs. The color bar scale shows the deviation of local polarization from the orientation of an applied electric field and circles represent OVs.

nant polarization $\bar{P}_{zr}$ decreases; whilst the reverse trends are observed for E_s, E_c and the dielectric loss W. Here W can be directly measured through the area of a hysteresis loop.

4 Discussion

The effect of OVs on ferroelectric properties of BTO can be traced back to distortion of cells near OVs. As shown in Figure 1(b), losing an oxygen ion destroys the neutral condition of two neighboring cells, and the distortion of cells results in the redistribution of ions near the OV. The infection propagates perpendicular to the [001] orientation as far as 5*a*, with *a* being the lattice constant of the perovskite cell, as shown in Figure 5(a). As a result, spontaneous polarization of these cells severely deviates from the [001] orientation, which causes reduction of their local polarization P_z. Thus, it is natural to see that, as shown in Figures 2 and 4, $\bar{P}_{zr}$ decreases with the increase of OV concentrations. The similar results were also reported in ref. [19].

Local polarization along the intersection between infected and non-distorted regions is unstable, which is sensitive to *E*. This is confirmed by the occurrence of the first hot spot at the intersection with a weaker *E* (0.25×10^7 V/m). In a single crystal system, however, local polarization is homogeneously distributed. Thus, a stronger *E* (1.75×10^7 V/m) is necessary to initiate the first hot spot (see Figure 3).

The OV-induced distortion of cells is irreversible. Spon-

taneous polarization of these cells can hardly be rectified in the [001] orientation. As shown in Figure 5(b), even if a system attains saturation, the area of distorted cells and the angle distribution of their polarizations remain almost unchanged. Thus, the difficulty to switch polarization of distorted cells leads to the increase of E_s, E_c and W. Since the distorted region has a characteristic length of 5a, two OVs with a distance over 5a can be regarded as isolated. Therefore, ferroelectric properties vary linearly with the concentration of isolated OVs. However, when the distance is less than 5a, distorted regions overlap mutually (see Figure 5(c)). This short distance does not induce the deviation of more local polarizations from the [001] orientation and thus ferroelectric properties are nonlinear, as shown in Figure 4. It is obvious that, whether isolated or not, OVs result in the increase of dielectric loss. To avoid such an unfavorable effect and save energy, a smart strategy is to treat a ferroelectric device with high-pressure oxygen annealing [10,11]. In this protocol, the OV sites can be occupied by oxygen and thus the dielectric loss is reduced [10].

5 Conclusions

In summary, molecular dynamics simulations have been performed to analyze the influence of OVs on ferroelectric behaviors of the tetragonal BTO phase. It is shown that the OV insertion causes the severe distortion of its neighboring cells. As a result, polarization of a distorted cell extremely deviates from [001], the direction of spontaneous polarization of a single crystal. This can hardly be altered by the applied external electric field even if a sample reaches saturation. To switch polarization of the distorted cell, stronger coercive and saturated fields are required in comparison with that of a non-distorted one, which leads to the increase of dielectric loss or the energy waste induced by OVs. This finding provides a good understanding on OV-affected hysteresis behaviors in ferroelectric ceramics.

This work was supported by the National Natural Science Foundation of China (Grant Nos. 11172024 and 11232013), the National Key Basic Research Program of China (Grant No. 2012CB937500), and the Research Grant Council of the Hong Kong Special Administrative Region, China (Grant No. 9042201 (CityU 11211015)). Computations were supported by resources provided by the Pawsey Supercomputing Centre with funding from the Australian Government and the Government of Western Australia, the LNMGrid of the State Key Laboratory of Nonlinear Mechanics and the ScGrid of Supercomputing Center, Computer Network Information Center of the Chinese Academy of Sciences.

1 Y. H. Zhang, J. W. Hong, B. Liu, and D. N. Fang, Nanotechnology **21**, 015701 (2010).
2 H. J. Song, T. Ding, X. L. Zhong, J. B. Wang, B. Li, Y. Zhang, C. B. Tan, and Y. C. Zhou, RSC Adv. **4**, 60497 (2014).
3 J. F. Scott, Science **315**, 954 (2007).
4 Y. H. Zhang, J. W. Hong, B. Liu, and D. N. Fang, Nanotechnology **20**, 405703 (2009).
5 D. N. Fang, and J. X. Liu, *Fracture Mechanics of Piezoelectric and Ferroelectric Solids* (Springer, Berlin, 2012).
6 J. Zhang, K. Xie, H. S. Wei, Q. Q. Qin, W. T. Qi, L. M. Yang, C. Ruan, and Y. C. Wu, Sci. Rep. **4**, 7082 (2014).
7 Z. Zhang, L. Lu, C. Shu, and P. Wu, Appl. Phys. Lett. **89**, 152909 (2006).
8 Q. Yang, J. X. Cao, Y. C. Zhou, Y. Zhang, Y. Ma, and X. J. Lou, Appl. Phys. Lett. **103**, 142911 (2013).
9 Q. Yang, J. X. Cao, Y. Ma, Y. C. Zhou, L. M. Jiang, and X. L. Zhong, J. Appl. Phys. **113**, 184110 (2013).
10 G. Subramanyam, M. W. Cole, N. X. Sun, T. S. Kalkur, N. M. Sbrockey, G. S. Tompa, X. M. Guo, C. L. Chen, S. P. Alpay, G. A. Rossetti Jr, K. Dayal, L. Q. Chen, and D. G. Schlom, J. Appl. Phys. **114**, 191301 (2013).
11 Y. Lin, D. Y. Feng, M. Gao, Y. D. Ji, L. B. Jin, G. Yao, F. Y. Liao, Y. Zhang, and C. L. Chen, J. Mater. Chem. C **3**, 3438 (2015).
12 S. Tinte, M. G. Stachiotti, S. R. Phillpot, M. Sepliarsky, D. Wolf, and R. L. Migoni, J. Phys. Condens. Matter **16**, 3495 (2004).
13 M. Sepliarsky, A. Asthagiri, S. R. Phillpot, M. G. Stachiottia, and R. L. Migoni, Curr. Opin. Solid State Mater. Sci. **9**, 107 (2005).
14 W. Humphrey, A. Dalke, and K. Schulten, J. Mol. Graphics. **14**, 33 (1996).
15 W. Smith, C. W. Yong, and P. M. Rodger, Mol. Simul. **28**, 385 (2002).
16 S. Nosé, Mol. Phys. **52**, 255 (1984).
17 W. G. Hoover, Phys. Rev. A **31**, 1695 (1985).
18 D. Wolf, P. Keblinski, S. R. Phillpot, and J. Eggebrecht, J. Chem. Phys. **110**, 8254 (1999).
19 Y. X. Chen, B. N. Liu, Y. Ma, and Y. C. Zhou, Nucl. Instrum. Meth. B **267**, 3090 (2009).